

6-1-2009

Hydrogel-based microsensors for wireless chemical monitoring

Ming Lei

Univ Minnesota, Dept Elect & Comp Engr

Antonio Baldi

Univ Minnesota, Dept Elect & Comp Engr

Eric Nuxoll

Univ Minnesota, Dept Pharmaceut

Ronald A. Siegel

Univ Minnesota, Dept Biomed Engr

Babak Ziaie

Birck Nanotechnology Center, Purdue University, bziaie@purdue.edu

Follow this and additional works at: <http://docs.lib.purdue.edu/nanopub>

 Part of the [Biomedical Engineering and Bioengineering Commons](#), and the [Nanoscience and Nanotechnology Commons](#)

Lei, Ming; Baldi, Antonio; Nuxoll, Eric; Siegel, Ronald A.; and Ziaie, Babak, "Hydrogel-based microsensors for wireless chemical monitoring" (2009). *Birck and NCN Publications*. Paper 353.

<http://docs.lib.purdue.edu/nanopub/353>

This document has been made available through Purdue e-Pubs, a service of the Purdue University Libraries. Please contact epubs@purdue.edu for additional information.

Hydrogel-based microsensors for wireless chemical monitoring

Ming Lei · Antonio Baldi · Eric Nuxoll ·
Ronald A. Siegel · Babak Ziaie

Published online: 12 March 2008
© Springer Science + Business Media, LLC 2008

Abstract We report fabrication and characterization of a new hydrogel-based microsensor for wireless chemical monitoring. The basic device structure is a high-sensitivity capacitive pressure sensor coupled to a stimuli-sensitive hydrogel that is confined between a stiff porous membrane

and a thin glass diaphragm. As small molecules pass through the porous membrane, the hydrogel swells and deflects the diaphragm which is also the movable plate of the variable capacitor in an LC resonator. The resulting change in resonant frequency can be remotely detected by the phase-dip technique. Prior to hydrogel loading, the sensitivity of the pressure sensor to applied air pressure was measured to be 222kHz/kPa over the range of 41.9–51.1MHz. With a pH-sensitive hydrogel, the sensor displayed a sensitivity of 1.16MHz/pH for pH3.0–6.5, and a response time of 45 minutes.

M. Lei · A. Baldi
Department of Electrical and Computer Engineering,
University of Minnesota,
Minneapolis, MN 55455, USA

E. Nuxoll · R. A. Siegel
Department of Pharmaceutics,
University of Minnesota,
Minneapolis, MN 55455, USA

R. A. Siegel
Department of Biomedical Engineering,
University of Minnesota,
Minneapolis, MN 55455, USA

B. Ziaie
School of Electrical and Computer Engineering,
Purdue University,
West Lafayette, IN 47907, USA

B. Ziaie (✉)
School of Electrical and Computer Engineering,
Birck Nanotechnology Center, Purdue University,
West Lafayette, IN 47907, USA
e-mail: bziaie@purdue.edu

Present address:
M. Lei
Intel Corp,
Chandler, AZ, USA

Present address:
A. Baldi
Centro Nacional de Microelectronica (CNM-IMB, CSIC),
Barcelona, Spain

Keywords Wireless sensor · Hydrogel · Pressure sensor ·
Chemical sensor · Smart material

1 Introduction

Environmentally sensitive hydrogels offer multiple opportunities in the design of biomedical microsystems (Siegel et al. 1988; Cao et al. 2001; Han et al. 2002; Gil and Hudson 2004; Kopecek 2003; Ziaie et al. 2004). These soft, three-dimensional cross-linked polymer networks swell and shrink in response to physical and chemical stimuli such as temperature, pH, and glucose concentration. Hence they are attractive candidates as components of chemical sensors and actuators operating in aqueous media (Kavanagh et al. 2004; Beebe et al. 2000; Shino et al. 1994; De et al. 2002). Integrating responsive hydrogels into MEMS and microfluidic structures enhances their function by providing solid scaffolds and movable structures against which the hydrogel can exert force. In addition, since response kinetics are governed either by molecular diffusion of analyte in the gel, or by cooperative diffusion of the hydrogel network, reducing hydrogel size from millimeter scale to, say, a

few tens of microns can speed up response from hours to seconds (response time scales quadratically with size).

Several microactuators responding to temperature, pH and glucose sensitive hydrogels have been reported. In-plane and out-of-plane flow can be started, stopped, or diverted by pH-regulated swelling and shrinking of the hydrogels. For example, Beebe et al. (2000) photopolymerized hydrogels around posts embedded in microchannels to create autonomous flow control. Gerlach et al. (2005) demonstrated on-off flow through a microcavity that could be switched on and off by expansion and contraction of a gel inside in response to pH change. Baldi et al. (2006) showed that flow across silicon devices can be regulated by stimuli-sensitive hydrogels polymerized around posts held in the center of cylindrical pores by narrow tethers. pH- and glucose-sensitive valves have been fashioned in which swelling and shrinking of the hydrogel against a compliant polydimethylsiloxane (PDMS) diaphragm opens or cuts off flow in a microchannel on the other side of the diaphragm (Baldi et al. 2003; Lei et al. 2007). Finally, hydrogel microlenses that change their depth of focus according to environmental conditions have been crafted (Dong et al. 2006).

There has also been growing interest in using chemically sensitive hydrogels in wireless microsensors for relevant physiological parameters, particularly glucose concentration. It is hoped that such sensors can be implanted with minimal surgical intervention and, after a short healing period, function without percutaneous breach by wire or optical fiber, and without need for battery power. Grimes et al. reported a thin-film microsensor for remote glucose monitoring using mass change of a swelling hydrogel to shift the mechanical resonant frequency of a magnetoelastic film (Grimes et al. 1999). Strong et al. (Strong et al. 2002) studied a capacitive sensor whose capacitance gap was controlled by hydrogel swelling. The variable capacitor was connected to an inductor, allowing monitoring of analyte concentration by tracking the shift in the resonant frequency of the circuit. However, this system was not integrated or miniaturized to permit implantation, and calcium nitrate, a non-physiological compound, was used as the model analyte. Building on the ideas introduced by Strong et al., and introducing a glucose-sensitive hydrogel containing methacrylamidophenylboronic acid (MPBA) side-chains (Shino et al. 1994; Alexeev et al. 2003; Kabilan et al. 2005), our group recently reported an integrated, implantable hydrogel/microresonator system sensitive to changes in glucose (Lei et al. 2006).

In this paper we present a number of technical details regarding construction of the device described in (Lei et al. 2006). We also illustrate the response of a device containing a pH-sensitive hydrogel. Design considerations related to device geometry and materials properties, which

could lead to future improvements, are outlined, and sources of variability which could limit sensor resolution are identified.

2 Analysis of factors affecting sensor design

The hydrogel/micromechanical chemical sensor is illustrated schematically in Fig. 1(a). A chemically sensitive hydrogel is confined between the top plate of a hermetically sealed microcapacitor, and a rigid porous membrane that permits diffusional exchange of analyte, water, and dissolved electrolytes. Osmotic swelling stresses generated in the hydrogel in response to changes in analyte concentration deflect the top capacitor plate, shifting the resonant frequency, $f = 1/2\pi\sqrt{LC}$, of an integrated circuit containing the microcapacitor (capacitance C) and a fixed micro-coil (inductance L).

Sensor sensitivity is determined by: (1) intrinsic sensitivity of the capacitive pressure sensor, and (2) the swelling pressure generated by the hydrogel in response to a change in the chemical environment. The capacitive sensor is expected to respond very rapidly to changes in swelling pressure, the dynamics of which is controlled by diffusional processes, as discussed below.

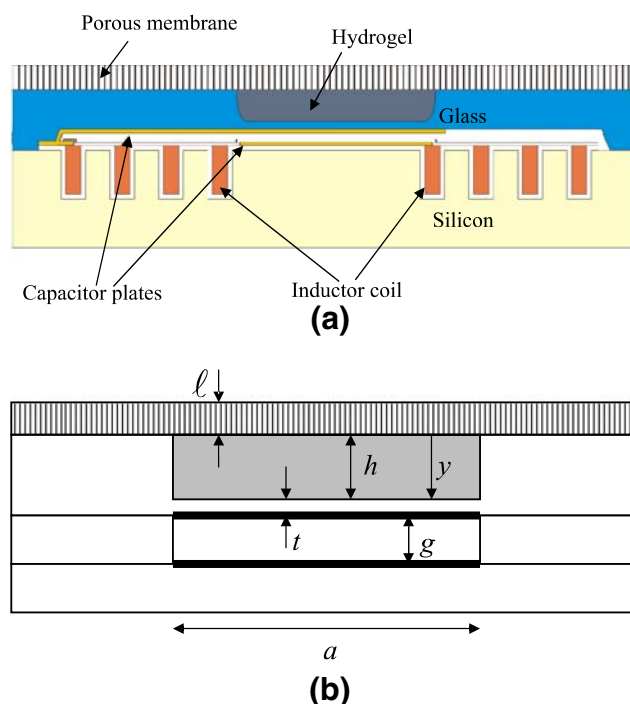


Fig. 1 Schematic drawing of the cross-section of the chemical sensor (a) and simplified structure with geometrical parameters (b)

2.1 Sensitivity and resolution of the capacitive sensor and microresonator

A dimensionless expression (Chau and Wise 1987) for capacitor sensitivity to pressure is based on the linear theory of bending plates (Den Hartog 1987)

$$\frac{\Delta C}{C_0} = \frac{Ka^4(1 - \nu^2)}{t^3g} \left(\frac{\Delta P}{E} \right) \tag{1}$$

where C_0 is the capacitance at zero pressure; ΔC is the change in capacitance due to pressure ΔP across the top (movable) plate; E and ν are the Young’s modulus and Poisson’s ratio of the capacitor plate; a and t are the plate span and thickness, g is the capacitor gap at zero pressure [Fig. 1(b)]; and K is a numerical shape factor ($K = 0.0746$ for square capacitor plates). Since the microinductor coil is of fixed geometry, sensitivity of the microresonator is given by $\Delta f/f_0 = -\Delta C/2C_0$. Sensitivity improves with a wide and thin top capacitor plate and a small gap between the plates. However, sensor dynamic range is inversely related to its sensitivity, as bending of the top plate ultimately leads to contact with the bottom plate. It should be mentioned that the thickness of the top plate can be reduced only so far as it resists fracture. Large bending of the plate can also result in a nonlinear response (Chau and Wise 1987).

While intrinsic transducer noise due to thermal fluctuation phenomena (Chau and Wise 1987) sets the lower theoretical limit for sensor resolution, noise in the readout circuitry sets higher practical limits. In the present system, readout was achieved by scanning the input impedance spectrum of an interrogating coil placed near the microresonator coil. At the resonant frequency a phase dip $\Delta\phi = \tan^{-1}(k^2Q_r)$ is observed, where k is the coupling coefficient between the two coils and Q_r is the quality factor of microresonator (Q_r ; Akar et al. 2001). Clearly, sensitivity and hence resolution of the device will be enhanced by optimizing these two characteristics.

The coil coupling coefficient depends primarily on the area occupied by the transponder coil. The small footprint of implantable MEMS-based transponders limits k to small values, often less than 1%. Increasing the quality factor by reducing resistive losses in the microresonator will sharpen the dip and make it easier to track its movement, therefore increasing resolution. The receiver noise floor, which depends on the equipment used for interrogation, is also important in setting the practical resolution.

2.2 Static response of the device to a change in analyte concentration

Pressure on the capacitor is the result of hydrogel swelling–deswelling in response to change in concentration of the

analyte. Precise analysis of the chemomechanical response of the hydrogel is difficult, insofar as deflection of the plate, and hence the thickness of the hydrogel in the swollen state, depends on distance from the center of the plate. Swelling pressure also decreases to some extent as the hydrogel expands. These complications can be neglected when membrane deflection is small compared to the thickness of the hydrogel. Comparing the hydrogel compartment thickness to the capacitor gap (Table 1), this condition is met in the present system. In the following static and dynamic analyses of swelling pressure response to changes in external analyte concentration, we assume that the hydrogel maintains a uniform thickness in position and time. In other words, we treat swelling pressure response as essentially isometric, although it is recognized that swelling pressure change is the main cause of membrane deflection.

Important attributes of the hydrogel are: (1) its volume fraction, ϕ_0 upon loading into its compartment; (2) the corresponding concentration of ionizable groups, σ_0 (mol/l H_2O); and (3) the fraction, α of those groups that are ionized in the presence of analyte. Assuming the external medium is an aqueous univalent salt (e.g. NaCl) solution of concentration c_s (mol/l H_2O), the mobile anion and cation concentrations inside the hydrogel fluid are given at equilibrium by λc_s and $\lambda^{-1}c_s$, respectively, where by λ is the Donnan ratio, set by the requirement of electrical neutrality inside the hydrogel, i.e.,

$$\left(\lambda - \frac{1}{\lambda} \right) c_s + z\alpha\sigma_0 = 0 \tag{2}$$

In this equality, z is the valence of ionized pendant group; $z = -1$ for acidic side-chains. Swelling pressure of the hydrogel is modeled by

$$\Delta P = \Delta P_0 + RT \left(\lambda + \frac{1}{\lambda} - 2 \right) c_s \tag{3}$$

where RT is the usual gas constant-temperature product (Rička and Tanaka 1984; Firestone and Siegel 1994). The term $\Delta P_0 = \Delta P_0(\phi_0)$ accounts for the polymer network’s elasticity and solvent compatibility, but does not depend on ionization. The second term in Eq. 3, to be denoted by $\Delta P'$, accounts for the net osmotic pressure of the mobile ions in

Table 1 Parameters of the fabricated glucose/pH sensor prototype

Parameter	Value (μm)
Rigid porous plate thickness (ℓ)	60
Hydrogel cavity thickness (h)	200
Diaphragm thickness (t)	30
Capacitor air gap (g)	20
Side of the square-shaped capacitor (a)	2,760

the hydrogel compared to the external medium, and combines the Donnan ratio with van't Hoff's law.

To complete the description of equilibrium swelling pressure, the fraction of ionizable groups that are ionized is specified. For an acidic, pH sensitive hydrogel,

$$\alpha = \frac{1}{1 + \lambda c_h / K_a} \tag{4}$$

where K_a is the acid dissociation constant of the side-chains (mol/l), and c_h is the external concentration of free hydrogen ions Setting $\text{pH} = -\log_{10}c_h$, and $\text{p}K_a = -\log_{10}K_a$, Eq. 4 is expressed in the more general and compact form

$$\alpha = \frac{1}{1 + \lambda / \lambda_{1/2}} \tag{5}$$

where $\lambda_{1/2} = 10^{\text{pH}-\text{p}K_a}$ is the value of λ at which the hydrogel reaches half its maximum ionization. The parameter K_g is infinite for the pH-sensitive hydrogel.

Combining Eqs. 2 and 5, we obtain the relation (with $z = -1$)

$$\lambda - \frac{1}{\lambda} = \frac{\sigma_0 / c_s}{1 + \lambda / \lambda_{1/2}} \tag{6}$$

The LHS of Eq. 6 increases monotonically and is positive for $\lambda > 1$, while the RHS decreases monotonically and is positive for $\lambda > 0$. As shown in Fig. 2, the two functions intersect at a single, equilibrium value $\lambda > 1$, which increases with

increasing σ_0 and pH, or with decreasing c_s , $\text{p}K_a$ and K_g , through the effect of these variables on λ . Also depicted in Fig. 2 is a means to read off $\Delta P'$, which increases monotonically for $\lambda > 1$ according to Eq. 3. For reference, at 37°C and $c_s = 155\text{mM}$ (physiologic ionic strength), $RTc_s = 3.94\text{atm}$, so in theory this device should be very sensitive to changes in pH or glucose concentration. Very similar analysis is possible for devices based on polybase gels (e.g. $z = +1$).

From the point of view of device design, this simplified model predicts that device sensitivity increases with increasing number of ionizable groups, and that sensitivity can be tuned by altering the $\text{p}K_a$ of those groups, when chemically possible. The model also suggests that physiological fluctuations in pH and ionic environment may be a source of “noise” which could limit the sensor's practical resolution.

2.3 Sensor temporal response

In the forgoing discussion of static swelling pressure, it was assumed that the device was in chemical and mechanical equilibrium, with uniform concentrations of solute, solvent and polymer components, and uniform charge state and stress throughout. Several concurrent and coupled processes determine the rate at which such equilibrium is achieved. These include: (1) diffusion of molecules, including analyte, salt ions, OH^- and H^+ through the rigid membrane; (2) diffusion of molecules inside the hydrogel; (3) reversible binding of certain molecules, including analyte, to ionizable sites; (4) development of local swelling pressure change due to change in ionization; and (5) mechanical readjustment of hydrogel to relax gradients in swelling pressure. These processes can be modeled by a set of coupled nonlinear partial differential equations (Eisenberg and Grodzinsky 1987; Grimshaw et al. 1990; English et al. 1997) which will be very complicated even with the simplifying assumptions that the hydrogel chamber's geometry is fixed, and that all gradients are in a single direction [y in Fig. 1(b)]. Some decoupling is possible by examining the response to small changes in analyte concentration. Even such a simplified analysis is beyond the scope of the present paper, however, and we merely make a few salient points.

First, it is reasonable to assume that reversible binding of molecules to the hydrogel, which alters its local fixed charge density, is rapid compared to diffusion of those chemicals through the rigid membrane and the hydrogel. When this is true, transport of molecules can be written in terms of the diffusion equation, with diffusion coefficients reduced from their corresponding bulk values due to obstructions and hydrodynamic interactions between the molecules and the hydrogel network (Amsden 1998; Masaro and Zhu 1999). Second, reversible binding slows

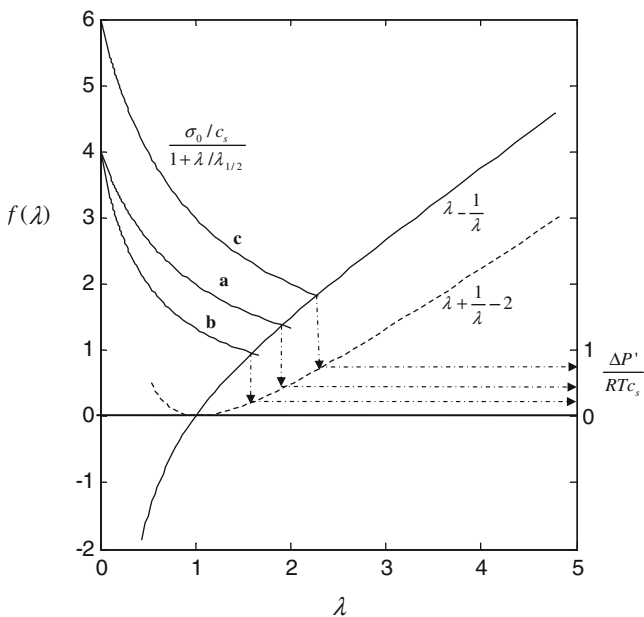


Fig. 2 Graphic solution of Eqs. 3 and 6. Solid monotonically increasing curve corresponds to the LHS of Eq. 6. Solid monotonically decreasing curves correspond to RHS of Eq. 6, with $\sigma_0/c_s = 4$, $\lambda_{1/2} = 1$ (a); $\sigma_0/c_s = 4$, $\lambda_{1/2} = 6$ (b); $\sigma_0/c_s = 6$, $\lambda_{1/2} = 1$ (c). Intersection of increasing and decreasing curves determines λ , which upon mapping onto dashed curve, gives the ionic portion of the change in swelling pressure

down diffusion (Crank 1975; Cussler 1997; Nussbaum and Grodzinsky 1981; Grimshaw et al. 1990). Third, mechanical response also obeys a diffusion equation, where the diffusion coefficient is the product of the longitudinal stiffness and the hydraulic (Darcy) permeability of the hydrogel network (Tanaka and Fillmore 1979; Grimshaw et al. 1990; Tomari and Doi 1994).

Since the governing equations are all of the diffusion type, and since natural boundary conditions (flux continuity) are expected to hold for all mobile species between the rigid membrane and the hydrogel, it follows that proportional scaling down of the thicknesses of these two structures should cause the chemical and mechanical relaxation times to decrease quadratically, provided external mass transfer limitations do not become prominent. (Thickness reduction is obviously limited by the ability of the membrane to withstand the hydrogel's swelling stress without fracturing.) Moreover, the hydrogel must be sufficiently thick that it can develop an adequate swelling pressure to flex the capacitor plate (see above).

As already indicated, static system sensitivity is predicted to improve with increasing density of fixed ionizable groups, σ_0 . However, increasing this density will slow down diffusion of binding molecules, and hence device response. Further, increasing σ_0 by “enriching” the hydrogel with more polymer (increasing ϕ_0) will decrease the rate of equilibration due to increased obstruction of flow of solvent and solutes.

3 Sensor fabrication and assembly

3.1 Prototype design features

A list of the geometrical parameters used for the prototype is provided in Table 1. These parameters were chosen based on the considerations in the previous section, but also based on ease of fabrication and availability of materials. Details of the structure and materials used for each device element are shown in Fig. 1(a).

The flexible diaphragm was machined from Pyrex glass. While silicon diaphragms are often used in micromachined pressure sensors (Chau and Wise 1987; Park et al. 1998; Akar et al. 2001), we chose Pyrex because of its relatively lower elastic modulus, 64GPa compared to 160GPa of (100) silicon (Beeby et al. 2004), which confers larger deflection and higher sensitivity. Pyrex glass also could be anodically bonded to the silicon substrate of the inductor. For the rigid membrane we used Anopore® (aluminum oxide porous membrane, from Whatman Inc., New Jersey) with 200nm pore diameter, 25% porosity and uniform thickness of 60 μ m. Aluminum oxide has a much larger

Young's modulus, 340GPa (Eugene 2005), than Pyrex glass. When the hydrogel swelled between the 60 μ m Anopore® membrane and the 30 μ m thick glass diaphragm used in the present microsensor, the membrane deflected much less than the diaphragm. Another advantage of Anopore® is its hydrophilicity which results in wetting and spreading of aqueous solution into the hydrogel cavity. Moreover, the pores of this material are sufficiently small to prevent diffusion of undesired species such as bacteria into the cavity.

The capacitor plates, made of a 0.5 μ m-thick gold layer, were divided into narrow strips by cut lines in order to reduce ohmic losses due to eddy currents. The gap between capacitor plates was 20 μ m. An oxide layer on top of the bottom plate prevented shorting of the plates for large deflections and allowed the pressure sensor to operate in touch mode, i.e., the pressure change could still be measured even though the top capacitor plate was deflected so far that parts of it touched the bottom plate. In this way, the working range of the pressure sensor could be extended, but this mode was not probed in the present work.

The microcoil was formed as a square spiral of copper-filled trenches embedded in silicon. Embedding (as opposed to surface printing) permitted the use of thicker copper layers and simplified the assembly with the other sensor parts. Optimization of the coil geometry was carried out using finite element analysis (Pan et al. 2005). Width and depth of the trenches were 30 and 50 μ m, respectively, while the separation of the copper lines was 20 μ m. The fabricated inductor had 20 turns, and the external side was 5mm.

3.2 Sensor fabrication

The sensor was batch fabricated from glass and silicon wafers using standard microfabrication techniques. Figure 3 shows the fabrication process for the chemical sensor, starting with a high-resistivity silicon wafer (resistivity $>10^4\Omega$ cm, from Kmbh Associates, CA). The high resistivity of the substrate reduced parasitic capacitance, thereby increasing the resonant frequency and quality factor of the sensor.

The embedded copper coil was formed by DRIE etch and electroplating processes, as shown in Fig. 3(a–c) (Pan et al. 2005). Coil inductance was 2.82 μ H. The bottom plate of the capacitor was formed by evaporating a Cr/Au (300/5,000Å) layer which was then lift-off patterned [Fig. 3(d)]. A PECVD oxide layer (1 μ m) was deposited and patterned on top of the bottom plate to insulate it from the top plate of the capacitor [Fig. 3(e)].

Fabrication of the glass member started with a Pyrex 7740 wafer (~250 μ m thick; Sensor Prep Services, IL) etched in a diluted HF/H₂O (4:1) solution to obtain a 20 μ m recess for the capacitor gap. A temporary air channel

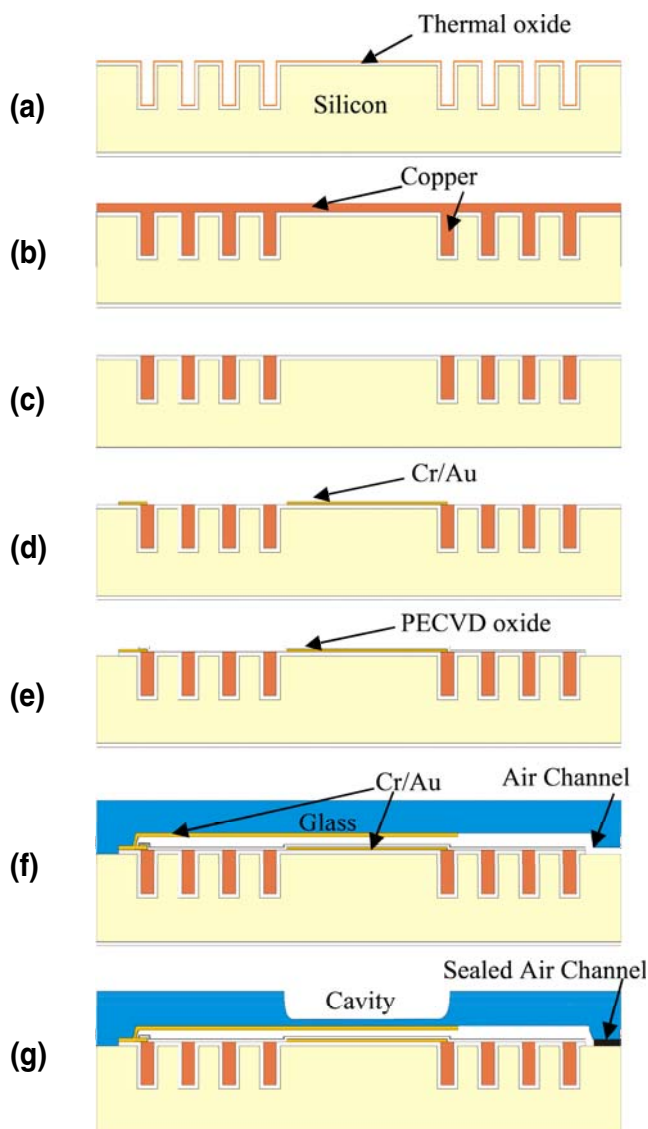


Fig. 3 Sequence of fabrication steps. (a) DRIE and thermal oxidation, (b) copper electroplating, (c) chemical mechanical polishing (CMP), (d) bottom Cr/Au patterning, (e) PECVD oxide deposition, (f) anodic bonding of glass wafer with patterned Cr/Au, (g) cavity etching

(150 μm wide) was simultaneously etched to the side of the capacitor. A Cr/Au (300/5,000 \AA) layer was then patterned in the glass recess to form the top plate of the capacitor [Fig. 3(f)].

The silicon and glass wafers were aligned to register the capacitor plates, with the gap inside, and the two wafers were anodically bonded at 380 $^{\circ}\text{C}$ and 900V to form an integrated LC resonator. Glass pillars were inserted near the plate perimeter to support the glass diaphragm and prevent collapse of the capacitor gap due to electrostatic forces during anodic bonding. The air channel relieved pressure gradients across the diaphragm during this step, and prevented a “lock-in” of diaphragm distortion. The outer side of the glass wafer was further etched to create a 200 μm -deep cavity for hydrogel loading [Fig. 3(g)].

The steps outlined above were carried out in batch, and the resulting assembly was diced into devices using a wafer saw. Individual devices were usually baked at 100 $^{\circ}\text{C}$ for 10min to eliminate residual water from the capacitor. After a device cooled down to room temperature, its air channel was sealed with viscous silicone rubber adhesive (DAP[®]: Dow Corning Corp., Midland, MI), to avoid future leaking of liquid into the capacitor gap. The wireless capacitive pressure sensor (microresonator) was then ready for characterization and hydrogel loading. Figure 4 shows a photograph of the microsensors next to a US penny.

3.3 Hydrogel loading and device assembly

The hydrogel was loaded *in situ* by polymerizing a slight excess of pre-gel solution in the sensor cavity. Under-loading of hydrogel could lead to a dead response zone. Pre-gel solution ($\sim 3 \mu\text{l}$) was dispensed in the cavity of the device and covered with a silanized glass plate on the top, with a 20- μm -thick aluminum foil spacer separating the two glass boundaries away from the cavity. The top glass plate's surface was rendered hydrophobic by silanizing with a 5vol.% solution of dichlorodimethylsilane (DCMS; Sigma-Aldrich) in toluene. This pretreatment prevented stiction of the hydrogel to the plate. Gelation was complete after 30min. The top plate was removed, and hydrogel extending outside the cavity was planed off with a razor blade. Finally, the Anopore[®] membrane was bonded to the glass substrate to cover the cavity, using a silicone-based adhesive. The sensors tested in the paper were of dimension $5 \times 5 \times 0.7 \text{mm}^3$, small enough for implantation.

The pH-sensitive hydrogel used in this study was a copolymer of methacrylic acid (MAA) and acrylamide (AAm). The pre-gel solution was composed of 167.5mg acrylamide, 50.0 μl methacrylic acid, 2.0 μl ethylene glycol dimethacrylate (EGDMA) as cross-linker, 25 μl *N,N,N',N'*-

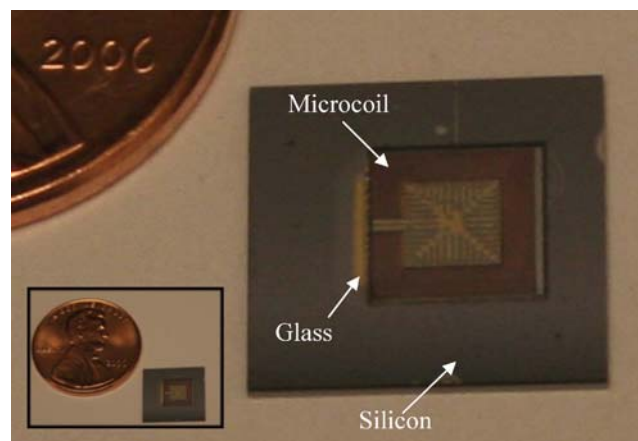


Fig. 4 Photograph of the microsensors next to a US penny

tetramethylethylenediamine (TEMED) as accelerator, and 1.1mg ammonium persulfate (APS) as initiator, all in 0.7ml of deionized water.

4 Results

4.1 Appearance and unloaded response

Optical micrographs of the glass and silicon parts before anodic bonding are displayed in Fig. 5. Two designs are shown. In Fig. 5(a), the top capacitor plate was continuously covered with metal, while in Fig. 5(b) features the cut lines introduced to reduce eddy currents and improve the quality factor.

The impedance spectrum of an external interrogating coil coupled to the microresonator, without hydrogel, was

measured with a HP4294A impedance analyzer (Agilent Technologies, CA). The external coil, 5mm in diameter and with five turns, was hand wound using a 0.25mm diameter insulated copper wire. This external coil was positioned 1mm away from the microcoil, with the two coils aligned coaxially. Figure 6(a) shows the resulting impedance phase spectrum of the external coil coupled with *LC* resonators, exposed to ambient external pressure. As mentioned before, the observed phase dip, $\Delta\phi$ coincided with the resonant frequency, ω_0 of the passive *LC* circuit.

Sensors with and without cut lines from the same fabrication batch showed different phase dips. Cut lines in the capacitor plates sharpened the phase dip by 95%, and improved the quality factor. Both of these effects led to improved resolution of the resonant frequency. The smaller capacitor plate area of sensors with cut lines resulted in a higher resonant frequency.

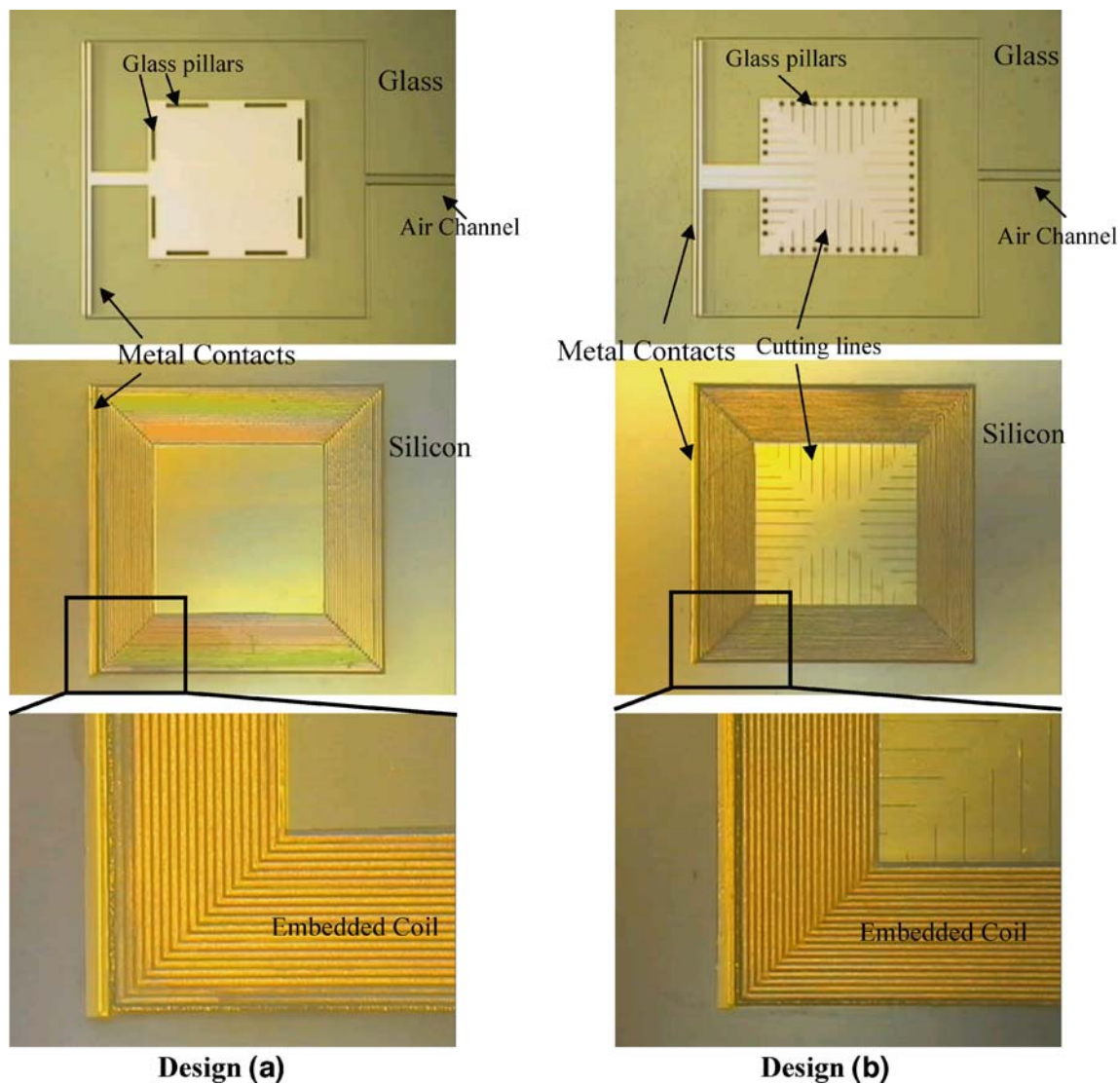
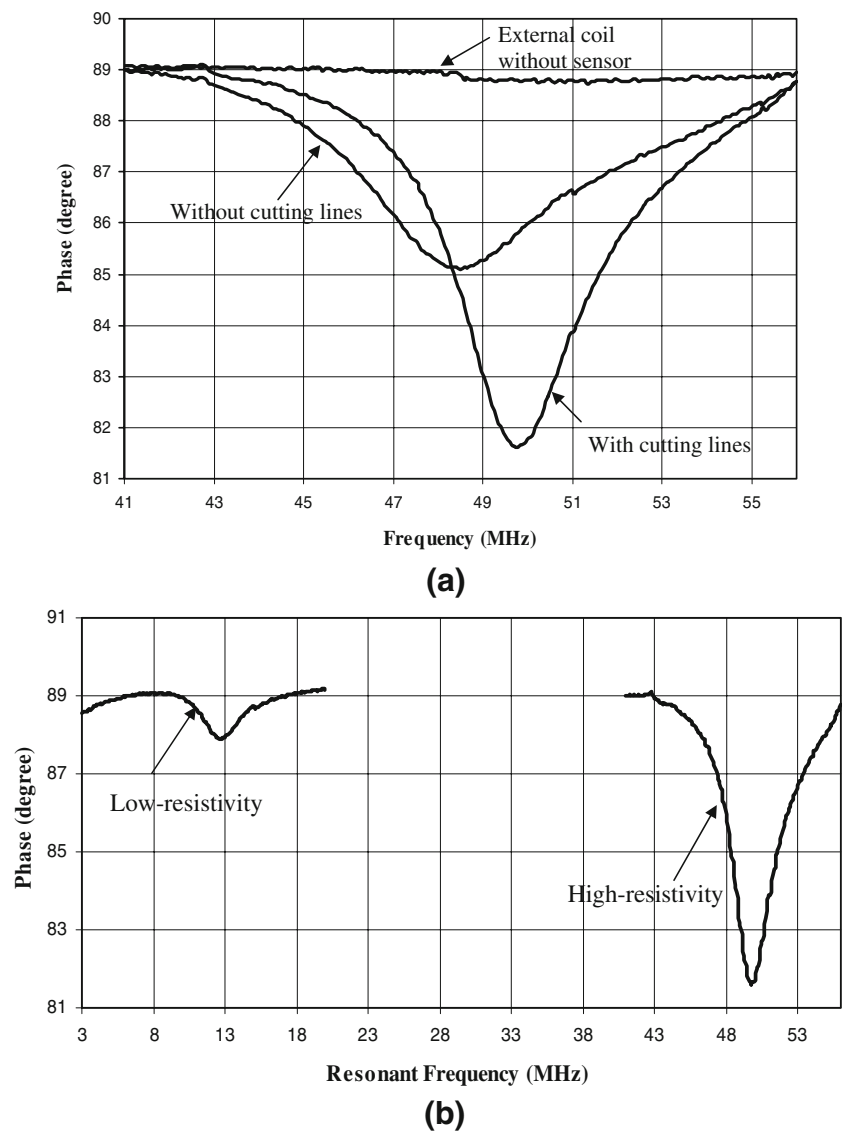


Fig. 5 Top views of the chemical sensor parts before anodic bonding (a) without cutting lines; (b) with cutting lines

Fig. 6 (a) Phase dips of pressure sensors with and without cutting lines, (b) comparison of the impedance curves of pressure sensors fabricated from low- and high-resistivity silicon wafers



Resistivity of the substrate embedding the inductor coil significantly affected the resonant frequency of the microresonator. A previously reported capacitive sensor based on a highly doped silicon wafer (resistivity 1–10 Ω cm; Pan et al. 2005) resonated at 12.8MHz [Fig. 6(a)], compared to 49.8MHz for the present sensor, which was constructed on a high-resistivity wafer [Fig. 6(b)]. The difference in resonant frequency is attributed to reduced parasitic capacitance, which is calculated to be 0.38 and 52.9pf in the high and low-resistivity wafers, respectively. Reducing parasitic capacitance enhances the relative contribution of variable capacitance, and higher sensitivity of the pressure sensor. The phase dip increased from 1.13° for the low-resistivity wafer to 7.31° for the high-resistivity wafer. Sharpness of the dip was also improved, making the detection of resonant frequency easier and more accurate.

4.2 Response to air pressure

Microresonator response to applied air pressure, again in the absence of hydrogel, was measured by clamping the device and pressurizing it with a syringe. Impedance spectra, resonant frequencies, and phase dips were determined as before, with the microresonator exposed to pressure range 0–6psi (0–41.4kPa). Resonant frequency shifted linearly with pressure, 222kHz/kPa, between 41.9 and 51.1MHz. This linear relation could be used to relate swelling pressure of the hydrogel embedded in the sensor, ΔP , to the measured resonant frequency.

4.3 Response to pH changes

The pH sensor, formed by polymerizing the mAA-co-AAm hydrogel inside the cavity, was hydrated in PBS buffer

solution of pH 7.4 and stored overnight to leach out unreacted chemicals and relax stress in the gel network. Testing was performed by immersing the sensor in PBS buffer solutions with different pH values. The device was equilibrated in each solution for at least 2 h before changing pH again.

Figure 7(a) shows the effect of pH on the sensor's resonant frequency, after equilibrium was established. The sensor's response range was pH 3.0–6.5, with sensitivity 1.16 MHz/pH at pH 5.0. The maximum hydrogel swelling pressure, 39.1 kPa measured at pH 7.4, is estimated to have deflected the 30- μm -thick glass diaphragm by about 10.2 μm at the center. This deflection is small enough to be considered within the elastic deformation range. Since the capacitor gap was 20 μm deep, the deflected diaphragm probably did not touch the bottom plate of the capacitor. The range over which the sensor showed its maximum sensitivity correlates with the range over which ionization of the hydrogel changes the most, since the pK_a of the incorporated methacrylic acid groups is close to 5.0.

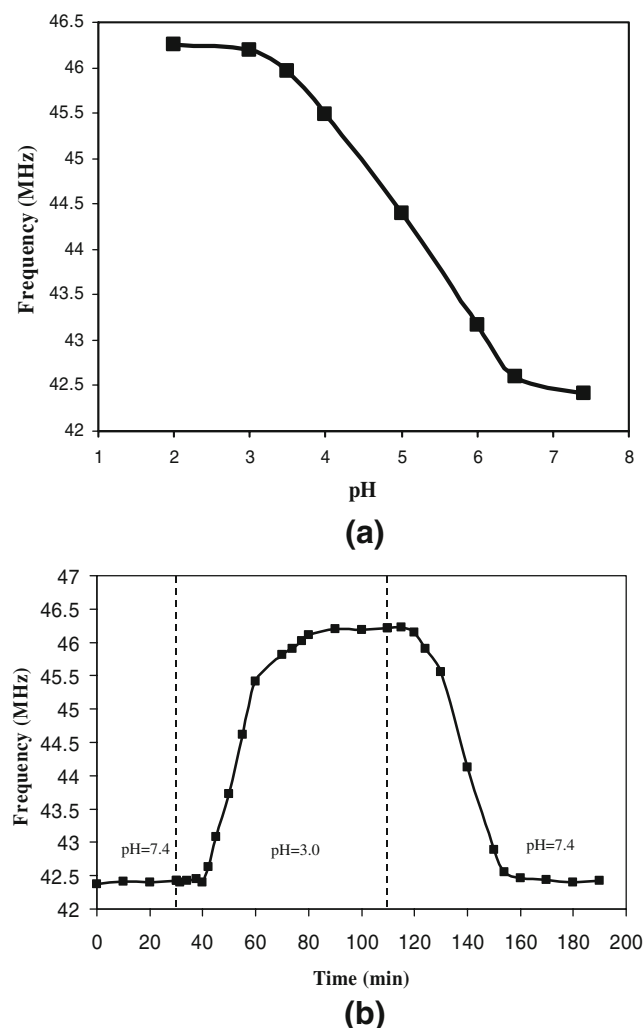


Fig. 7 (a) Remotely measured resonant frequency versus pH, (b) resonant frequency response to alternating pH solutions of 3.0 and 7.4

Increasing pH lead to increased charge, increased swelling pressure, increased deflection, and therefore decreased resonant frequency.

Figure 7(b) displays the kinetics of response of the sensor to pH change, between pH 7.4 and 3.0, and back. After a relatively short (~10 min) dead time, pressure equilibrated after 40–45 min in both directions. The initial dead time was probably due to diffusional lag of H^+ ions crossing the Anopore[®] membrane, and the subsequent kinetics of swelling pressure response were probably controlled by diffusion and binding/release of H^+ in the hydrogel, along with mechanical relaxation of the hydrogel chains in response to changes in local charge density (Eisenberg and Grodzinsky 1987; Grimshaw et al. 1990; English et al. 1997).

5 Discussion and conclusions

This paper demonstrates the principle of remote chemical sensing using a microresonator coupled through its capacitor to a hydrogel whose swelling pressure responds to changes in analyte concentration. The resonant frequency detection principle is simple and amenable to design changes, either by altering geometric properties of the microresonator components and the hydrogel, or by changing the hydrogel's chemical composition.

Little effort was expended to optimize the response time, and it is clear that the present device responds rather sluggishly. As noted above, response time is expected to improve quadratically as the thicknesses are simultaneously scaled down. The hydrogel cavity in the present prototype was 200 μm deep, and this thickness can be reduced substantially, as can the thicknesses of the glass diaphragm supporting the upper capacitor plate, and the rigid microporous membrane. Of course, these size reductions must be carried out such that the solid components do not fracture in the face of hydrogel swelling pressures, and such that adequate frequency resolution is maintained when the device, now of reduced size, is interrogated by the external coil.

While H^+ was the model “analyte” used in the present studies, the principles apply to similarly constructed sensors for other molecules. For example, our earlier reported work for glucose sensing with MPBA hydrogels showed sufficient sensitivity (34.3 kHz/mM over the range 0–20 mM glucose) for practical applications (Lei et al. 2006). In addition to the obvious need to study sensor stability and viability *in vivo* (Alcantar et al. 2000; Sharkawy et al. 1997), it will be necessary to develop hydrogels that are specific to the molecule being detected in order to minimize interference by other species that may be present in the physiological environment (Alexeev et al. 2003; Kabilan et al. 2005; Mujumdar 2007).

Acknowledgements The authors thank the staff of the Nanofabrication Center (NFC) of the University of Minnesota for their assistance. Many thanks go to Tingrui Pan, Woohyek Choi, Hao Hou, Yuandong Gu, and Zhihua Li for their valuable suggestions. Funding for this project was provided by US Army Medical Research Acquisition Activity DA/DAMD17-02-1-0722 and by the National Institutes of Health, grant EB003215.

References

- O. Akar, T. Akin, K. Najafi, *Sens. Actuators A* **95**, 29 (2001)
- N.A. Alcantar, E.S. Aydil, J.N. Isrealachvili, *J. Biomed. Mater. Res.* **51**, 343 (2000)
- V.L. Alexeev et al., *Anal. Chem.* **75**, 2316 (2003)
- B. Amsden, *Polym. Gels Netw.* **6**, 13 (1998)
- A. Baldi, Y. Gu, P.E. Loftness, R.A. Siegel, B. Ziaie, *Journal of Microelectromechanical Systems* **12**, 613 (2003)
- A. Baldi, M. Lei, Y. Gu, R.A. Siegel, B. Ziaie, *Sens. Actuators, B, Chem.* **114**, 9 (2006)
- D.J. Beebe, J.S. Moore, J.M. Bauer, Q. Yu, R.H. Liu, C. Devadoss, B.-H. Jo, *Nature* **404**, 588 (2000)
- S. Beeby, G. Ensell, M. Kraft, N. White, *MEMS Mechanical Sensors* (Artech House Inc., Norwood, 2004)
- X. Cao, S. Lai, L.J. Lee, *Biomedical Microdevices* **3**, 109 (2001)
- H.L. Chau, K.D. Wise, *IEEE Trans. Electron. Devices*, **34**, 850 (1987)
- J. Crank, *The Mathematics of Diffusion* (Cambridge University Press, Oxford, 1975)
- E.L. Cussler, *Diffusion* (Cambridge University Press, Cambridge, 1997)
- S.K. De, N.R. Aluru, B.B.J. Johnson, W.C. Crone, D.J. Beebe, J. Moore, *Journal of Microelectromechanical Systems* **9**, 544 (2002)
- J.P. Den Hartog, *Advanced Strength of Materials* (Dover Publishing, NY, 1987)
- L. Dong, A.K. Agarwal, D.J. Beebe, H. Jiang, *Nature* **442**, 551 (2006)
- S.R. Eisenberg, A.J. Grodzinsky, *J. Biomech. Eng.* **109**, 79 (1987)
- A. English, T. Tanaka, E.R. Edelman, *J. Chem. Phys.* **107**, 1645 (1997)
- I.A. Eugene, *Electronic Materials Science* (Wiley, Hoboken, 2005)
- B.A. Firestone, R.A. Siegel, *J. Biomater. Sci. Polym. Ed.* **43**, 901 (1994)
- G. Gerlach, M. Guenther, J. Sorber, G. Suchanek, K.-F. Arndt, A. Richter, *Sens. Actuators. B.* **111–112**, 555–561 (2005)
- E.S. Gil, S.M. Hudson, *Prog. Polym. Sci.* **29**, 1173–1222 (2004)
- C.A. Grimes, D. Kouzoudis, K.G. Ong, R. Crump, *Biomedical Microdevices* **2**, 51 (1999)
- P.E. Grimshaw, J.H. Nussbaum, M.L. Yarmush, A.J. Grodzinsky, *J. Chem. Phys.* **93**, 4462 (1990)
- I.S. Han, M.H. Han, J. Kim, S. Lew, Y.J. Lee, F. Horkay, J.J. Magda, *Biomacromolecules* **3**, 1271 (2002)
- S. Kabilan et al., *Biosens. Bioelectron.* **20**, 1602 (2005)
- C.A. Kavanagh, Y.A. Rochev, W.M. Gallagher, K.A. Dawson, A.K. Keenan, *Pharmacol. Ther.* **102**, 1 (2004)
- J. Kopecek, *Eur. J. Pharm.* **20**, 1 (2003)
- M. Lei, A. Baldi, E. Nuxoll, R.A. Siegel, B. Ziaie, *Diabetes Technol. Ther.* **8**, 112 (2006)
- M. Lei, B. Ziaie, E. Nuxoll, K. Ivan, Z. Noszticzus, R.A. Siegel, *J. Nanosci. Nanotech.* **7**, 780 (2007)
- L. Masaro, X.X. Zhu, *Prog. Polym. Sci.* **24**, 731 (1999)
- S. Mujumdar, Ph.D. Thesis. (University of Minnesota, 2007)
- J.J. Nussbaum, A.J. Grodzinsky, *J. Membr. Sci.* **8**, 193 (1981)
- T. Pan, A. Baldi, E. Davies-Venn, R.F. Drayton, B. Ziaie, *J. Micromech. Microeng.* **15**, 849 (2005)
- E. Park, J. Yoon, E. Yoon, *Jpn. J. Appl. Phys.* **37**, 7124 (1998)
- J. Rička, T. Tanaka, *Macromolecules* **17**, 2916 (1984)
- A.D. Sharkawy, B. Klitzman, G.A. Truskey, W.M. Reichert, *Frese-nius' J. Anal. Chem.* **366**, 402 (1997)
- D. Shino, K. Kataoka, Y. Koyama, M. Yokoyama, T. Okano, Y. Sakurai, *J. Intell. Mater. Syst. Struct.* **5**, 311 (1994)
- R.A. Siegel, M. Falamarzian, B.A. Firestone, B.A. Moxley, *J. Control. Release* **8**, 179 (1988)
- Z.A. Strong, A.W. Wang, C.F. McConaghy, *Biomedical Microdevices* **4**, 97 (2002)
- T. Tanaka, D. Fillmore, *J. Chem. Phys.* **70**, 1214 (1979)
- T. Tomari, M. Doi, *J. Phys. Soc. Jpn.* **63**, 2093 (1994)
- B. Ziaie, A. Baldi, M. Lei, Y. Gu, R.A. Siegel, *Adv. Drug Deliv. Rev.* **56**, 145 (2004)